LETTER

doi:10.1038/nature11573

Observation of entanglement between a quantum dot spin and a single photon

W. B. Gao[1], P. Fallahi[1], E. Togan[1], J. Miguel-Sanchez[1] & A. Imamoglu[1]

Entanglement has a central role in fundamental tests of quantum mechanics[1] as well as in the burgeoning field of quantum information processing. Particularly in the context of quantum networks and communication, a main challenge is the efficient generation of entanglement between stationary (spin) and propagating (photon) quantum bits[2]. Here we report the observation of quantum entanglement between a semiconductor quantum dot spin and the colour of a propagating optical photon. The demonstration of entanglement relies on the use of fast, single-photon detection, which allows us to project the photon into a superposition of red and blue frequency components. Our results extend the previous demonstrations of single-spin/single-photon entanglement in trapped ions[3], neutral atoms[4,5] and nitrogen–vacancy centres[6] to the domain of artificial atoms in semiconductor nanostructures that allow for on-chip integration of electronic and photonic elements[7,8]. As a result of its fast optical transitions and favourable selection rules, the scheme we implement could in principle generate nearly deterministic entangled spin–photon pairs at a rate determined ultimately by the high spontaneous emission rate. Our observation constitutes a first step towards implementation of a quantum network with nodes[9] consisting of semiconductor spin quantum bits[10–12].

Recent advances have demonstrated the potential of semiconductor spin quantum bits (qubits) in the implementation of fast, single-qubit[13–16] and two-qubit[17] quantum gates. Realization of a large-scale, spin-based quantum information processor, however, remains an outstanding challenge owing to limitations on the coherent coupling of distant qubits. An alternative route is provided by the concept of distributed quantum computation, which involves small-scale, few-qubit quantum processor nodes interconnected by single photons that are quantum correlated with spin qubits[18]. Remarkably, photonic circuits allowing for efficient optical-photon-based quantum communication between the nodes can be fabricated on the same semiconductor chip[7]. For this distributed approach to solid-state quantum information processing, as well as for long-distance quantum communication, generation of the spin–photon entanglement that we demonstrate here emerges as a key enabling technology.

Our experiments utilize a single-electron-charged, self-assembled InGaAs quantum dot. Figure 1a shows the relevant energy-level diagram as well as the allowed optical transitions in Voigt geometry, where an external magnetic field (B_x) is applied perpendicular to the growth direction[19]. In our scheme, it is possible to generate and verify high-fidelity entanglement for $0.2\,\mathrm{T} \leq B_x \leq 1\,\mathrm{T}$: the lower limit ensures that the quantum dot is optically excited only to the red trion state, $|T_r\rangle$ (Fig. 1a), and the upper limit is dictated by the detector time resolution. In our experiments, we choose $B_x = 0.7$ T. All four transitions between the two ground states and the two excited states (Fig. 1a) have identical oscillator strengths and are linearly polarized either parallel (H) or perpendicular (V) to the applied field direction[19]. The ground states of the quantum dot are identified by the orientation of the electron spin, with $|\uparrow\rangle$ and $|\downarrow\rangle$ respectively denoting spins parallel and antiparallel to the magnetic field direction. Spontaneous emission of an H- or V-polarized photon at frequency ω_{red} or, respectively, ω_{blue} from the trion state $|T_r\rangle$ at rate $\Gamma/2$ brings the quantum dot back into the state $|\downarrow\rangle$ or, respectively, $|\uparrow\rangle$. In addition to resonant laser excitation of the trion states, our scheme uses non-resonant, right-hand-circularly (σ^+)-polarized, 4-ps-long mode-locked laser pulses that are red-detuned from the trion transitions by ~210 GHz: these pulses induce a coherent rotation of the electron spin, with minimal trion excitation[13]. We depict these pulses in Fig. 1a with a time-dependent effective magnetic field along the z direction (Supplementary Information).

The basic principle behind the deterministic generation of a spin–photon entangled state is straightforward: following the excitation of the quantum dot into the trion state, the radiative recombination projects the coupled quantum dot/photonic mode system into the entangled state

$$|\Psi\rangle = \frac{1}{\sqrt{2}}(|\downarrow\rangle|\omega_{\mathrm{red}};\mathrm{H}\rangle + i|\uparrow\rangle|\omega_{\mathrm{blue}};\mathrm{V}\rangle) \quad (1)$$

written in the computational basis, where $|\omega_{\mathrm{red}};\mathrm{H}\rangle$ and $|\omega_{\mathrm{blue}};\mathrm{V}\rangle$ denote propagating single-photon-pulse state vectors with respective centre frequencies ω_{red} and ω_{blue} and respective polarizations H and V. The electronic Zeeman energy satisfies $\omega_Z = \omega_{\mathrm{blue}} - \omega_{\mathrm{red}}$.

We use resonance fluorescence measurements[20,21] to map the optical transitions of the quantum dot. Observation of resonance fluorescence from the quantum dot transitions in Voigt geometry requires the presence of a second laser field that rotates the electron spin, because otherwise spin pumping, which takes place within a few nanoseconds[19], ensures that the quantum dot remains dark to optical excitation. To characterize the quantum dot, we use a pulse sequence where two resonant laser pulses, respectively 5 and 1.2 ns long, are applied in addition to a 4-ps pulse implementing spin rotation (Fig. 1b). The resonance fluorescence spectrum that we obtain as we scan the resonant laser across the four allowed quantum dot transitions is depicted in Fig. 1c. Our fast, single-photon detection capability allows us to monitor the time dependence of the resonance fluorescence: as Fig. 1d shows, we can easily distinguish photons that are emitted during excitation by the resonant laser both from those emitted as a result of (unwanted) trion excitation induced by the π-pulse and the background photons from the 4-ps laser. This ability to monitor photons generated in definite time windows is crucial for the verification of spin–photon entanglement. The experimental set-up that allows us to implement two-laser excitation as well as selective detection of resonance fluorescence generated in different time windows or at different frequencies, or both, is depicted in Fig. 1e (Methods Summary). Suppression of the σ^+-polarized background laser light is ensured by a polarizer[21] that projects the polarization of the transmitted resonance fluorescence photons to σ^- (left-hand circular). Because the spin polarization correlations are erased at this stage, entanglement is between the electron spin orientation and the centre frequency of the single-photon pulse (such that the photonic states can be written as $|\omega_{\mathrm{red}}\rangle$ and $|\omega_{\mathrm{blue}}\rangle$).

To demonstrate spin–photon entanglement, we first prepare the quantum dot in state $|\uparrow\rangle$ with a probability exceeding 87% by applying a 5-ns resonant laser field tuned to the $|\downarrow\rangle \leftrightarrow |T_r\rangle$ transition; we refer to

[1]Institute of Quantum Electronics, ETH Zurich, CH-8093 Zurich, Switzerland.

©2012 Macmillan Publishers Limited. All rights reserved

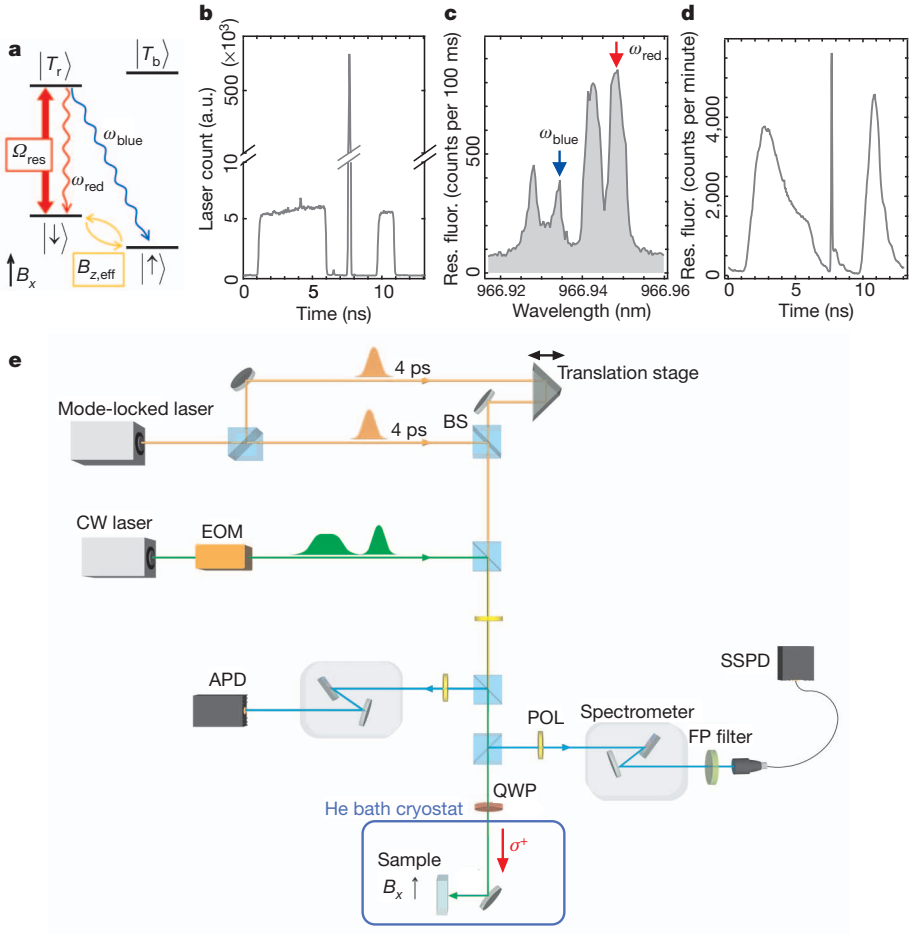

Figure 1 | Quantum dot transitions and experimental set-up. a, The energy-level diagram of a single-electron-charged InGaAs quantum dot in Voigt geometry. Spontaneous emission following resonant optical excitation of the trion state, $|T_r\rangle$, with Rabi frequency Ω_{res} leads to the generation of an entangled spin–photon state. Non-resonant, σ^+-polarized, 4-ps laser pulses implement coherent spin rotation; the effect of such a laser pulse is equivalent to a time-dependent magnetic field, $B_{z,eff}$, that is perpendicular to the external field B_x (Supplementary Information). **b**, The pulse sequence used to characterize the quantum dot transitions: following a 5-ns resonant laser excitation, a 4-ps π-pulse is applied. A 1.2-ns resonant laser excitation completes the pulse sequence, which has a repetition period of 13 ns. a.u., arbitrary units. **c**, Resonance fluorescence spectrum generated by the pulse sequence depicted in **b** as the laser frequency ω_L is scanned across the quantum dot transitions at $B_x = 0.7$ T. **d**, Time dependence of resonance fluorescence obtained when the laser is on resonance with the $|\downarrow\rangle \leftrightarrow |T_r\rangle$ transition ($\omega_L = \omega_{red}$), indicated by the red arrow in **c**. The spike that coincides with the 4-ps laser pulse is due to incomplete suppression of reflected laser photons. **e**, The schematic of the experimental set-up highlighting the important optical elements. BS, beam splitter; CW, continuous wave; EOM, electro-optic modulator; FP, Fabry–Pérot; POL, polarizer; QWP, quarter-wave plate.

this laser as the measurement/preparation pulse. We then transfer the quantum dot to the $|\downarrow\rangle$ state using a 4-ps π-pulse[13]. An entangled spin–photon pair is then generated by exciting $|T_r\rangle$ with a 1.2-ns resonant laser pulse, which we refer to as the entanglement pulse; the corresponding pulse sequence is depicted in Fig. 2a. The whole pulse sequence is repeated after 13 ns, with the 5-ns resonant laser implementing spin measurement for the preceding pulse sequence as well as ensuring spin pumping/preparation in the $|\uparrow\rangle$ state for the subsequent cycle (Fig. 2a). The fact that the average number of photons emitted during this spin measurement/pumping time window is ~1, together with our relatively modest combined collection and detection efficiency of ~0.1%, implies that we extract heralded spin information[22]; that is, the unlikely event of a photon being detected at the avalanche photodiode (APD) tells us with very high confidence level that the spin (before the measurement) is $|\downarrow\rangle$, whereas the absence of a detection event yields no information. An additional π-pulse (Fig. 2a, dashed curve) applied 3 ns after the onset of the entanglement pulse enables a photon detection event at the APD during the measurement/preparation pulse to project the spin into $|\uparrow\rangle$ rather than $|\downarrow\rangle$.

Figure 2b shows the time-resolved resonance fluorescence at frequencies ω_{blue} and ω_{red}. The depicted resonance fluorescence starts at the onset of the entanglement pulse, which we take to be $t = 0$ in Figs 2 and 3. For all experiments depicted in Fig. 2, we use a Fabry–Pérot interferometer to select out photons either at ω_{blue} or ω_{red} before sending them to the superconducting single-photon detector (SSPD). The (unconditional) resonance fluorescence counts at the two frequencies are nearly identical in intensity, indicating that the two decay channels have equal oscillator strengths. The shape of these single-photon pulses is determined by the time dependence of the trion population, which in turn is determined by the excitation laser (through its pulse shape and the Rabi frequency, Ω_{res}) and the spontaneous emission time $\Gamma^{-1} = 650$ ps. Figure 2c (green bars) shows the normalized, zero-time-delay photon autocorrelation function, $g^{(2)}(0) = 0.02 \pm 0.01$, for photons emitted during the time interval [1.2 ns, 1.64 ns] (Fig. 2b, dashed green box). This measurement demonstrates that the unlikely two-photon emission events lead to a small degradation of the entanglement. When we measure photon correlations for the whole single-photon pulse, we find that $g^{(2)}(0) = 0.16 \pm 0.01$ (Fig. 2c, black bars). This value is limited partly by a residual contribution from the reflected laser photons and partly by multiple excitation of the quantum dot during the entanglement pulse. We note that verifying the spin–photon entanglement in the time interval [1.2 ns, 1.64 ns] also allows us to

©2012 Macmillan Publishers Limited. All rights reserved

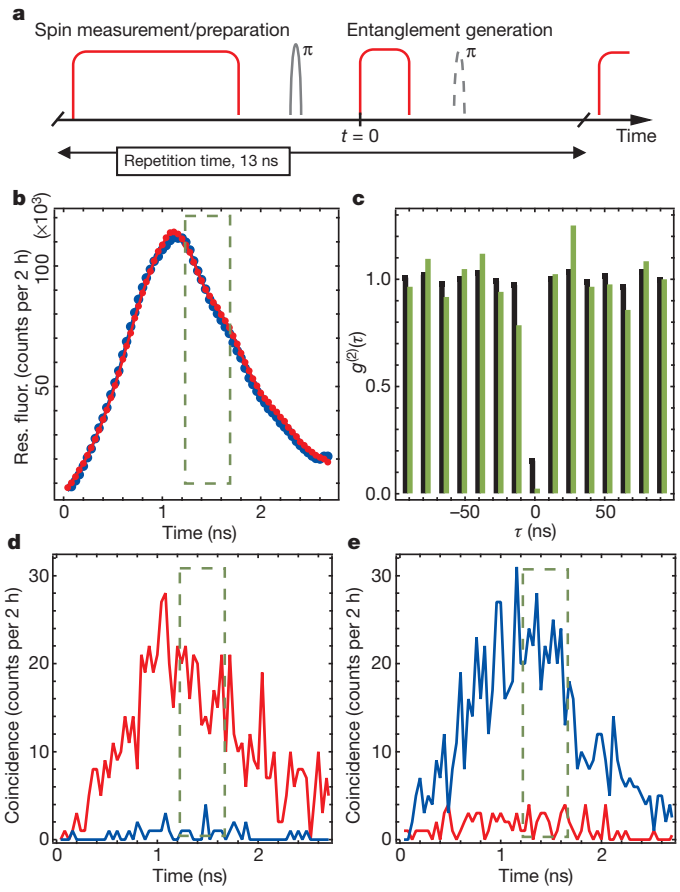

Figure 2 | Measurement of classical spin–photon correlations. **a**, The pulse sequence used to measure the spin–photon correlations in the computational (non-rotated) basis. A 5-ns laser excitation resonant with the $|\downarrow\rangle \leftrightarrow |T_r\rangle$ transition implements spin pumping/preparation in $|\uparrow\rangle$; detection of a resonance fluorescence event during this measurement/preparation pulse projects the spin state to $|\downarrow\rangle$. Following a 4-ps-long π-pulse, a 1.2-ns laser, resonant with the $|\downarrow\rangle \leftrightarrow |T_r\rangle$ transition, initiates the generation of an entangled spin–photon pair. An additional π-pulse (dashed curve) is applied only to obtain the data shown in **e**. **b**, Time-resolved resonance fluorescence obtained at ω_{red} (red) and ω_{blue} (blue) using the pulse sequence shown in **a**: identical intensities and pulse shapes at the two frequencies indicate that the detected events stem from a single trion state ($|T_r\rangle$) and that the oscillator strength of the transitions at ω_{red} and ω_{blue} are identical. **c**, Photon correlation measurement carried out on resonance fluorescence generated in a 3-ns time window starting at the onset of the entanglement pulse ($t = 0$). The observed $g^{(2)}(0) = 0.16$ (black) is limited by background laser photons. When we carry out photon correlation measurements on photons detected during the time interval [1.2 ns, 1.64 ns] (box in **b**), we find that $g^{(2)}(0) = 0.02$ (green). **d**, Time-dependent resonance fluorescence at ω_{red} (red) and ω_{blue} (blue), conditioned on detection of a photon during the subsequent measurement/preparation pulse. The strong suppression of conditional photon detection events at ω_{blue} demonstrates the strong classical correlation between spin measurement yielding $|\downarrow\rangle$ and a photon detection at ω_{red}. **e**, Same as in **d** but now with a π-pulse applied before the measurement/preparation pulse, showing strong correlations between spin detection in $|\uparrow\rangle$ and photon detection at ω_{blue}.

avoid the effects of the fluctuating nuclear spin environment on the entanglement fidelity.

Demonstration of spin–photon correlations in the computational/non-rotated basis requires the measurement of classical correlation between the spin direction and the photon frequency. This is achieved by carrying out a coincidence measurement between resonance fluorescence photons at either ω_{blue} or ω_{red} generated immediately after the entanglement pulse and those generated during the measurement/preparation pulse. Conditional on the detection of the spin state $|\downarrow\rangle$, we find that the probability of detecting a blue (ω_{blue}) photon at the SSPD is drastically suppressed compared with the probability of detecting a red (ω_{red}) photon (Fig. 2d). The ratio of the red to blue photons in the time interval [1.2 ns, 1.64 ns] is ~21:3. To quantify completely the classical correlations in the computational basis, we introduce a 4-ps π-pulse at $t = 3$ ns that makes it possible to condition the single-photon colour measurements on detection of the spin in $|\uparrow\rangle$. In this case, we find that the red-photon detection events are strongly suppressed (Fig. 2e). The ratio of the blue to red photons in this case, however, is only ~10:3, owing to (unwanted) trion excitation by the 4-ps laser that leads to lower fidelity in the subsequent spin measurement. From these two measurements, we determine the fidelity of the classical correlations to be $F_1 = 0.87 \pm 0.09$ (Supplementary Information).

To verify that the generated spin–photon state is entangled, we next show that the correlations between spin orientation and photon colour exist in a rotated basis[6]. In the rotated basis, the relative phase between the two components of the entangled state in equation (1) is crucial. After generation at time t_g, the two components acquire a time-dependent phase that stems from the different propagation phase factors of the blue and red frequency components of the photonic mode. In our experiments, we infer the generation time from the detection time, t_d, of the single photon at the SSPD, through the relation $t_g = t_d - L/c$, where L denotes the distance from the quantum dot to the detector and c is the speed of light. Hence, given a photon detection event at t_d, we can a-posteriori write the time dependence of the spin–photon entangled state of equation (1) as

$$|\Psi(t)\rangle = \frac{1}{\sqrt{2}}\left(|\downarrow\rangle|\omega_{red};\mathrm{H}\rangle e^{-i\omega_Z(t-t_g)} + i|\uparrow\rangle|\omega_{blue};\mathrm{V}\rangle\right)$$

The requisite spin measurement is implemented by rotating the quantum dot electron spin with either a π/2-pulse or a 3π/2-pulse at $t = t_1 = 1.7$ ns. A photon detection event at the APD during the following measurement/preparation pulse then projects the electron spin into $(|\downarrow\rangle - i|\uparrow\rangle)/\sqrt{2}$ (π/2-pulse) or $(|\downarrow\rangle + i|\uparrow\rangle)/\sqrt{2}$ (3π/2-pulse). The photonic wavefunction consistent with the spin measurement after the π/2-pulse can be written as $\left(|\omega_{red};\mathrm{H}\rangle e^{-i\omega_Z(t_1-t_g)} - |\omega_{blue};\mathrm{V}\rangle\right)/\sqrt{2}$ (Supplementary Information). After passing through the polarizer, which fixes the polarization of the photon to be $(|\mathrm{H}\rangle - i|\mathrm{V}\rangle)/\sqrt{2}$, this wavefunction is

$$|\tilde{\Phi}\rangle = \frac{1}{\sqrt{2}}\left(|\omega_{red}\rangle e^{-i\omega_Z(t_1-t_g)} - i|\omega_{blue}\rangle\right) \quad (2)$$

In the experiment, we remove the Fabry–Pérot interferometer and directly send the single-photon pulses onto a fast SSPD[23] with a jitter of $\Delta\tau = 60$ ps. With a SSPD that had jitter smaller than $1/\omega_Z$, we could determine t_g well enough to resolve the time dependence in equation (2), which in turn would indicate that the photonic state is projected into a superposition of its two frequency components. The resulting coincidence probability is $P \approx [1 + \sin(\omega_Z(t_1 - t_g))]/2$. As a consequence of the time-dependent relative phase, two single-photon states generated at different times, t_g^a and t_g^b, such that $\omega_Z(t_g^a - t_g^b) = \pi$, allow us to infer the overlap of the photonic state with two orthogonal states. Random photon detection times together with the fact that the single-photon pulse width, τ, satisfies $\omega_Z\tau > 1$, allow us effectively to implement projective measurements into orthogonal states such as $|\omega_{red}\rangle \pm |\omega_{blue}\rangle$.

Figure 3b shows the coincidence between the single-photon detection events induced by the entanglement pulse and the detection of a photon during the measurement/preparation pulse, following a π/2-pulse: the oscillations with a period given by $2\pi/\omega_Z = 238$ ps in the conditioned single-photon detection events (Fig. 3b, red squares) are in stark contrast to the unconditioned single-photon detection events shown in Fig. 2b. This particular time dependence, stemming from the conditioned photonic wavefunction given in equation (2), constitutes a remarkable manifestation of the quantum coherence of

©2012 Macmillan Publishers Limited. All rights reserved

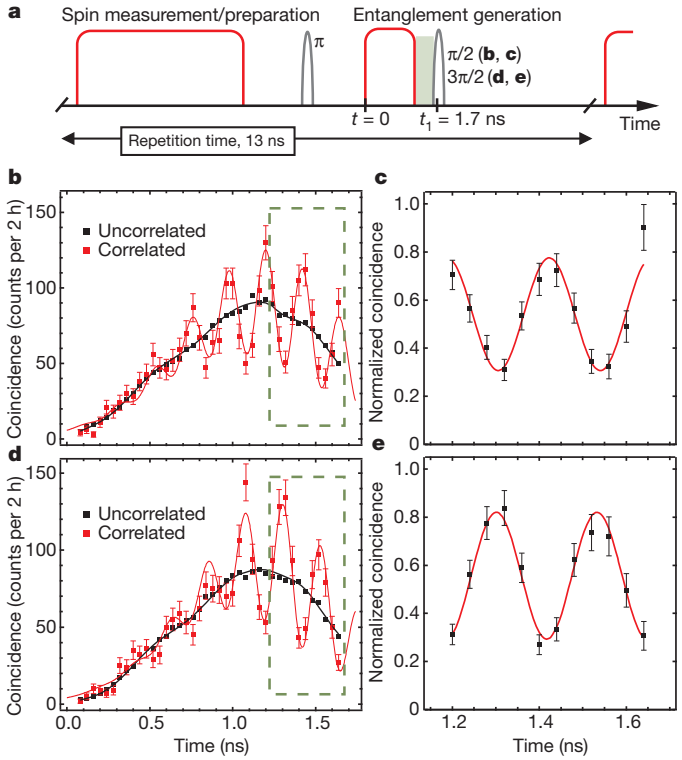

Figure 3 | Demonstration of quantum correlation between the electron spin and the emitted single-photon pulse. **a**, The pulse sequence used to measure the spin–photon correlations in the rotated basis: the only difference from Fig. 2a is the introduction of a $\pi/2$- or $3\pi/2$-pulse, applied at $t = 1.7$ ns, that rotates the spin measurement basis such that the detection of a photon during the subsequent measurement/preparation pulse projects the spin to $|\downarrow\rangle - i|\uparrow\rangle$ or, respectively, $|\downarrow\rangle + i|\uparrow\rangle$. The shading indicates the [1.2 ns, 1.64 ns] entanglement analysis time window. **b**, Time-resolved coincidence events between the single-photon detection following the entanglement pulse and the detection of a photon during the first measurement/preparation pulse following a $\pi/2$-pulse (red squares). For comparison, an average of coincidence events between the spin and photon detection events taking place in 25 different excitation/preparation cycles is also shown (black squares). The red curve is a fit to the experimental data, and the black curve is the rescaled single-photon pulse shown in Fig. 2b. **c**, Normalized coincidence during the [1.2 ns, 1.64 ns] window (box in **b**); normalization is carried out by dividing the number of counts from correlated spin–photon pairs by twice the number of uncorrelated events in the corresponding time bin. **d**, Same as in **b** but now with a $3\pi/2$-pulse. **e**, Same as in **c** but now with a $3\pi/2$-pulse. All error bars represent 1 s.d., deduced from Poissonian statistics of the raw detection events.

the entangled spin–photon system. For comparison, we also show an average of coincidence events between the spin and photon detection events taking place in different excitation/preparation cycles (Fig. 3b, black squares). As expected, these coincidences do not show any oscillations, but they help us quantify the degree of quantum correlation. Normalizing the coincidence detection between correlated spin–photon pairs and focusing on the time interval between 1.2 and 1.64 ns, we find a visibility of about $45 \pm 6\%$ for the observed oscillations (Fig. 3c). Figure 3d shows the time-dependent coincidence measurements obtained by applying a $3\pi/2$-pulse before the measurement/preparation pulse. Figure 3e in turn shows that when we focus on the same time interval, the oscillations for spin detection along $(|\downarrow\rangle + i|\uparrow\rangle)/\sqrt{2}$ (Fig. 3e) are π out of phase relative to those along $(|\downarrow\rangle - i|\uparrow\rangle)/\sqrt{2}$ (Fig. 3c) and have a visibility of $47 \pm 4\%$. The actual coincidence detection rate in the detection time window [1.2 ns, 1.64 ns] is 240 counts per hour. Using the data from Fig. 3c, e, we determine the fidelity of the quantum correlations in this rotated basis to be the average of these two visibilities, yielding $F_2 = 0.46 \pm 0.04$ (Supplementary Information). The overall measured entanglement fidelity is then $F \geq (F_1 + F_2)/2 = 0.67 \pm 0.05$, limited predominantly by the finite jitter of the SSPD.

A major limitation in the demonstration of quantum correlations between the electron spin and the photon frequency stems from the relatively short ground-state spin decoherence time, T_2^*, of the electron spin, originating from the slowly fluctuating nuclear spin environment. The decay of the oscillations as a function of $t_1 - t_g$ in conditioned single-photon detection events (Fig. 3b, d) constitutes a measurement of the electron spin decoherence that was previously carried out using Ramsey interferometry[24]. By fitting the decay of coincidence measurements in the time window [0 ns, 1.64 ns] we find that $T_2^* = 1.1 \pm 0.2$ ns for the data in Fig. 3b and that $T_2^* = 0.9 \pm 0.2$ ns for the data in Fig. 3d, for this quantum dot.

In our experiments, the extraction efficiency of the spin–photon entanglement (that is, the fraction of emitted photon collected by the objective) is ~0.1. We emphasize, however, that near-deterministic generation of entanglement is possible using InGaAs quantum dots: several groups have demonstrated that quantum dot emissive properties can be drastically improved by incorporating them in tailored photonic nanostructures[7,25,26]. The fraction of photons emitted at the zero-phonon line typically exceeds 90% in self-assembled quantum dots; enhanced radiative recombination rate in devices with Purcell factors much greater than one ensures that the fraction of photons emitted at the zero-phonon line approaches unity[8]. By embedding a quantum dot in a micropillar cavity yielding a Purcell factor exceeding one, it is also possible to ensure single-photon collection efficiency approaching unity[26].

Our results realize the long-standing goal of establishing a light–matter quantum interface in optically active quantum dots in GaAs-based materials[2,11]. Integration of self-assembled or other optically active quantum dots with spin qubits in electrically gated quantum dots[12] would allow entangled spin–photon pairs to be used to entangle distant spin qubits. The relatively short T_2^* observed in our experiment presents a limitation on the separation of distant spin qubits that can be entangled. We emphasize that methods for narrowing the fluctuating Overhauser field[27] could be used to increase T_2^*. Implementing such a scheme before spin–photon entanglement generation or using spin-echo techniques would extend the distance limit set by T_2^*. Observation of indistinguishable photons from two distant, self-assembled quantum dots in a Hong–Ou–Mandel interferometer, which was demonstrated experimentally[28,29], constitutes an additional key step towards realization of distant-spin entanglement. We emphasize that coincidence detection in a Hong–Ou–Mandel set-up that signals successful entanglement swapping can be implemented in a straightforward way using photons from two spin–frequency entangled pairs[30].

METHODS SUMMARY

Experimental set-up. Two time-delayed 4-ps pulses from a mode-locked laser are combined with a 5-ns pulse and a 1.2-ns pulse obtained from a continuous-wave laser using an electro-optic modulator, and the resulting single beam is sent to the quantum dot. The relative delay of the 4-ps pulses can be changed with a translation stage. A polarizer and a quarter-wave plate ensure that the lasers are σ^+-polarized at the quantum dot. Emitted quantum dot photons are detected by an APD and a SSPD through two collection paths. In each path, a combination of a polarizer and a spectrometer suppresses the reflected laser background. A Fabry–Pérot filter is used to select the colour of the entanglement photon for the computational basis measurements and is removed for the rotated basis measurements.
Synchronization. In the experiment, the fixed repetition rate of a mode-locked laser is used as a reference to synchronize the time delay of experimental pulses and also to synchronize the time of detection events. The repetition rate is measured using a fast photodiode (40-ps rise time). The 32nd harmonic of the repetition rate is extracted with a band-pass filter centred at 2.4 GHz, amplified (70 dB gain) and then fed into the clock input of a pulse-pattern generator (PPG), which is used to synchronize both the pulse generation and the detection circuitries. An electrical pulse output from the PPG is used to drive an electro-optic modulator, modulating a single-mode continuous-wave laser and ensuring that the spin measurement/preparation pulses and entanglement-generation pulses are always in a fixed time order. Another output of the PPG is used to pre-scale the 2.4-GHz

©2012 Macmillan Publishers Limited. All rights reserved

synchronization signal, before being fed into the clock input of a time-correlated single-photon-counting module. This module records the time delay of photon arrival events (via the APD or the SSPD) relative to the pre-scaled clock.

Received 7 June; accepted 10 September 2012.

1. Aspect, A., Grangier, P. & Roger, G. Experimental realization of Einstein-Podolsky-Rosen-Bohm gedanken experiment: a new violation of Bell's inequalities. *Phys. Rev. Lett.* **49,** 91–94 (1982).
2. DiVincenzo, D. P. The physical implementation of quantum computation. *Fortschr. Phys.* **48,** 771–783 (2000).
3. Blinov, B., Moehring, D. & Duan, L. Observation of entanglement between a single trapped atom and a single photon. *Nature* **428,** 153–157 (2004).
4. Volz, J. *et al.* Observation of entanglement of a single photon with a trapped atom. *Phys. Rev. Lett.* **96,** 030404 (2006).
5. Wilk, T., Webster, S. C., Kuhn, A. & Rempe, G. Single-atom single-photon quantum interface. *Science* **317,** 488–490 (2007).
6. Togan, E. *et al.* Quantum entanglement between an optical photon and a solid-state spin qubit. *Nature* **466,** 730–734 (2010).
7. Hennessy, K. *et al.* Quantum nature of a strongly coupled single quantum dot-cavity system. *Nature* **445,** 896–899 (2007).
8. Faraon, A. *et al.* Coupling of nitrogen-vacancy centers to photonic crystal cavities in monocrystalline diamond. *Phys. Rev. Lett* **109,** 033604 (2012).
9. Yuan, Z.-S. *et al.* Experimental demonstration of a BDCZ quantum repeater node. *Nature* **454,** 1098–1101 (2008).
10. Loss, D. & DiVincenzo, D. P. Quantum computation with quantum dots. *Phys. Rev. A* **57,** 120–126 (1998).
11. Imamoğlu, A. *et al.* Quantum information processing using quantum dot spins and cavity QED. *Phys. Rev. Lett.* **83,** 4204–4207 (1999).
12. Hanson, R. *et al.* Spins in few-electron quantum dots. *Rev. Mod. Phys.* **79,** 1217–1265 (2007).
13. Press, D., Ladd, T. D., Zhang, B. & Yamamoto, Y. Complete quantum control of a single quantum dot spin using ultrafast optical pulses. *Nature* **456,** 218–221 (2008).
14. Greilich, A. *et al.* Ultrafast optical rotations of electron spins in quantum dots. *Nature Phys.* **5,** 262–266 (2009).
15. Poem, E. *et al.* Accessing the dark exciton with light. *Nature Phys.* **6,** 993–997 (2010).
16. Kim, D. *et al.* Ultrafast optical control of entanglement between two quantum-dot spins. *Nature Phys.* **7,** 223–229 (2011).
17. Shulman, M. D. *et al.* Demonstration of entanglement of electrostatically coupled singlet-triplet qubits. *Science* **336,** 202–205 (2012).
18. Cirac, J., Ekert, A. & Huelga, S. Distributed quantum computation over noisy channels. *Phys. Rev. A* **59,** 4249–4254 (1999).
19. Xu, X. *et al.* Fast spin state initialization in a singly charged InAs-GaAs quantum dot by optical cooling. *Phys. Rev. Lett.* **99,** 097401 (2007).
20. Muller, A. *et al.* Resonance fluorescence from a coherently driven semiconductor quantum dot in a cavity. *Phys. Rev. Lett.* **99,** 187402 (2007).
21. Vamivakas, A. N., Zhao, Y., Lu, C.-Y. & Atature, M. Spin-resolved quantum-dot resonance fluorescence. *Nature Phys.* **5,** 198–202 (2009); corrigendum **5,** 925 (2009).
22. Yılmaz, S. T., Fallahi, P. & Imamoglu, A. Quantum-dot-spin single-photon interface. *Phys. Rev. Lett.* **105,** 033601 (2010).
23. Gol'tsman, G. N. *et al.* Picosecond superconducting single-photon detector. *Appl. Phys. Lett.* **79,** 705–707 (2001).
24. Press, D. *et al.* Ultrafast optical spin echo in a single quantum dot. *Nature Photon.* **4,** 367–370 (2010).
25. Claudon, J. *et al.* A highly efficient single-photon source based on a quantum dot in a photonic nanowire. *Nature Photon.* **4,** 174–177 (2010).
26. Dousse, A. *et al.* Ultrabright source of entangled photon pairs. *Nature* **466,** 217–220 (2010).
27. Xu, X. *et al.* Optically controlled locking of the nuclear field via coherent dark-state spectroscopy. *Nature* **459,** 1105–1109 (2009).
28. Flagg, E. B. *et al.* Interference of single photons from two separate semiconductor quantum dots. *Phys. Rev. Lett.* **104,** 137401 (2010).
29. Patel, R. *et al.* Two-photon interference of the emission from electrically tunable remote quantum dots. *Nature Photon.* **4,** 632–635 (2010).
30. Moehring, D. L. *et al.* Entanglement of single-atom quantum bits at a distance. *Nature* **449,** 68–71 (2007).

Supplementary Information is available in the online version of the paper.

Acknowledgements We acknowledge discussions with W. Chin, M. Kroner, A. Srivastava, J. Elzerman, A. Reinhard, T. Volz, P. Maletinsky and D. Gershoni. This work is supported by NCCR Quantum Science and Technology, a research instrument of the Swiss National Science Foundation; the Swiss NSF (grant no. 200021-140818); an ERC Advanced Investigator Grant (A.I.); and a Marie Curie International Incoming Fellowship within FP7 (W.B.G.).

Author Contributions All authors contributed extensively to this work.

Author Information Reprints and permissions information is available at www.nature.com/reprints. The authors declare no competing financial interests. Readers are welcome to comment on the online version of the paper. Correspondence and requests for materials should be addressed to W.B.G. (weibo@phys.ethz.ch) or A.I. (imamoglu@phys.ethz.ch).

©2012 Macmillan Publishers Limited. All rights reserved